Nuclear Engineering and Technology 55 (2023) 330–338

Contents lists available at ScienceDirect

Nuclear Engineering and Technology

journal homepage: www.elsevier.com/locate/net

Original Article

Possible power increase in a natural circulation Soluble-Boron-Free Small Modular Reactor using the Truly Optimized PWR lattice

Steven Wijaya, Xuan Ha Nguyen, Yonghee Kim*

Department of Nuclear and Quantum Engineering, Korea Advanced Institute of Science and Technology (KAIST), 291 Daehak-ro, Yuseong-gu, Daejeon, 34141, Republic of Korea

ARTICLE INFO

Article history:
Received 27 April 2022
Received in revised form
1 September 2022
Accepted 4 September 2022
Available online 9 September 2022

Keywords:
Small modular reactor
Soluble-Boron-free (SBF)
Natural circulation
Truly Optimized PWR (TOP) Lattice
NuScale

ABSTRACT

In this study, impacts of an enhanced-moderation Fuel Assembly (FA) named Truly Optimized PWR (TOP) lattice, which is modified based on the standard 17 × 17 PWR FA, are investigated in a natural circulation Soluble-Boron-Free (SBF) Small Modular Reactor (SMR). Two different TOP lattice designs are considered for the analysis; one is with 1.26 cm pin pitch and 0.38 cm fuel pellet radius, and the other is with 1.40 cm pin pitch and 0.41 cm fuel pellet radius. The NuScale core design is utilized as the base model and assumed to be successfully converted to an SBF core. The analysis is performed following the primary coolant circulation loop, and the reactor is modelled as a single channel for thermal-hydraulic analyses. It is assumed that the ratio of the core pressure drop to the total system pressure drop is around 0.3. The results showed that the reactor power could be increased by 2.5% and 9.8% utilizing 1.26/0.38 cm and 1.40/0.41 cm TOP designs, respectively, under the identical coolant inlet and outlet temperatures as the constraints.

1. Introduction

Recently, Small Modular Reactors (SMRs) have become an attractive option in the global nuclear industries. Both heat exchanger and steam generator are integrated inside the reactor pressure vessel, enhancing reactor safety [1]. Furthermore, eliminating complicated reactivity control systems such as the Chemical and Volume Control System (CVCS) makes the reactor system simpler and more compact. In spite of the several advantages, soluble boron has several well-known drawbacks, such as potentially positive Moderator Temperature Coefficient (MTC) at a high soluble boron concentration, a large volume of radioactive liquid waste, material corrosion, and crud accumulation [2,3]. Moreover, the Soluble-Boron-Free (SBF) condition enhances the passive autonomous load-follow, including frequency control operation [4,5]. The SMR safety is improved further by utilizing the passive cooling system [6]. Therefore, a natural circulation SBF SMR becomes an appealing option for next-generation reactors.

Recently, a Truly Optimized PWR (TOP) lattice has been demonstrated to successfully enhance the neutronic performance of an SBF SMR named Autonomous Transportable On-demand reactor Module (ATOM) [7]. In the TOP design of Ref. 7, the pin pitch is enlarged to increase the hydrogen-to-uranium (HTU) number density ratio enhancing the neutron moderation. In addition, the reactor safety is enhanced further by utilizing Cr15Al-coated Zircaloy-4 as the Accident Tolerant Fuel (ATF) cladding with negligible change in the excess reactivity, radial, and axial power distribution [8].

In the natural circulation SMR, the coolant mass flow rate is relatively lower than that of the pump-cooled SMR. The core mass flow rate is determined by the balance of the primary cooling system driving force and resistance force [9]. The reactor power, geometrical design of the reactor system, and the operation state of the heat exchanger influence the passively cooled reactor thermal-hydraulic performance [10].

In this study, the impacts of the TOP lattice design on a natural circulation SBF SMR core are investigated to maximize the reactor power. The NuScale reactor, a soluble-boron SMR, is utilized as the base model design [11]. It is assumed that the NuScale core can be successfully converted to an SBF core. Several studies have demonstrated the feasibility of the passive cooled SBF SMR based on the NuScale core design utilizing the TOP lattice [12,13]. In this preliminary study, a single channel model is utilized to model the reactor thermal-hydraulically. The impacts of TOP lattice on the

* Corresponding author.
E-mail address: yongheekim@kaist.ac.kr (Y. Kim).

https://doi.org/10.1016/j.net.2022.09.003

core pressure drop, system mass flow rate, and reactor power under the constraint of identical inlet and outlet temperatures are investigated. It will serve as the preliminary bases for the further comprehensive study and motivation for designing the natural circulation SBF SMR utilizing the TOP lattice. An in-house code based on several mathematical models for the natural circulation system is developed for the analysis.

This paper is organized as follows, Section 2 describes the TOP lattice configurations, while the calculation model, correlations, and assumptions are described in Section 3. Section 4 presents the NuScale reactor key parameters and the numerical results. Finally, Section 5 concludes the investigation.

2. Truly Optimized PWR (TOP) Lattice

In the current Fuel Assembly (FA) design for PWRs, the fuel lattice is clearly under-moderated and optimized under the soluble-boron condition to assure a negative MTC during the reactor operation. By eliminating the soluble boron, the HTU ratio can be increased further, resulting in a softer neutron spectrum and higher excess reactivity. The softer neutron spectrum results in always sufficiently negative and similar MTC throughout the operational cycle, which is favorable for a smaller temperature defect and larger cold shutdown margin at highly burned conditions [14]. Fig. 1 shows the infinite multiplication factor as a function of the HTU of two fuel enrichments.

Based on the standard 17 × 17 FA, there are two approaches to enhance the neutron moderation. The first approach is by enlarging the pin pitch while fixing the fuel radius, and the second one is by reducing the fuel radius while preserving the FA size. In this study, both TOP lattice designs are considered. The fuel pin pitch is enlarged to 1.4 cm in the first design without changing the fuel pellet radius as in Ref. 7. Consequently, the equivalent core radius increases due to the enlarged pin pitch. The impact of the TOP lattice with varied fuel pin pitches on the power of the natural circulation core has been investigated [15]. On the other hand, the fuel pellet radius is reduced to 0.38 cm with the fixed 1.26 pin pitch in the second design, as shown in Fig. 2. Therefore, the core size does not change in the second design. Thus, the second TOP design is preferable when the TOP lattice is adopted in the existing commercial PWRs. However, the fuel inventory decreases due to the reduced fuel pellet radius in the second design. Consequently, the specific power density may increase proportionally. It should be noted that in South Korea, the smaller fuel radius was used commercially in the Kori reactor unit-2 [16].

3. Calculation models

In this study, the analysis is performed under the steady-state condition of the primary coolant circulation loop. Furthermore, the coolant flow in the reactor core is modelled as a single channel without considering any cross-flows between the fuel assemblies.

3.1. Pressure drop models in primary loop

The one-dimensional steady-state primary loop momentum [9] equation is written as follows:

$$\Delta p_{pump} - \Delta p_{loss} + \Delta p_{Buoyancy} = 0, \tag{1}$$

where Δp_{pump} is the pressure head provided by the pump, Δp_{loss} is the total pressure drop around the entire loop, and $\Delta p_{buoyancy}$ is the buoyancy pressure head. In the natural circulation system, $\Delta p_{pump} = 0$ as the coolant is driven by the density differences between the hot and cold legs (buoyancy force). Therefore, Eq. (1) becomes:

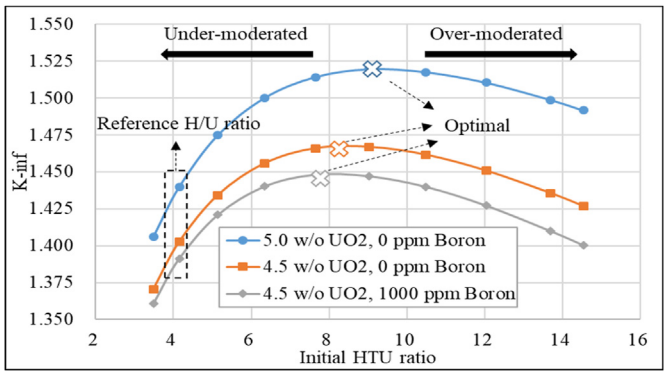

Fig. 1. Infinite multiplication factor with respect to HTU value [14].

$$\Delta p_{loss} = \Delta p_{Buoyancy}. \tag{2}$$

The right-hand side of Eq. (2) is the buoyancy force, which is the driving force of the natural circulation system and is derived by integrating the gravitational term in the coolant momentum equation over the flow path along the primary natural circulation loop using the Boussinesq approximation as follows:

$$\Delta p_{Buoyancy} = (\rho_{cold} - \rho_{hot}) g \Delta H, \tag{3}$$

where ρ_{cold} is the coolant density at the cold leg, ρ_{hot} is the coolant density at the hot leg, g is the gravity acceleration constant, and ΔH is the thermal center difference between the reactor core and Primary Heat Exchanger (PHX). The left-hand side of Eq. (2) is the summation of all irreversible pressure drops (i.e., pressure drops due to wall friction and form losses) in the primary circulation loop. Therefore, the total pressure drop is defined as:

$$\Delta P_{loss} = \Delta P_{lowplenum} + \Delta P_{core} + \Delta P_{riser} + \Delta P_{topplenum} + \Delta P_{steamgenerator} + \Delta P_{downcomer}, \tag{4}$$

where $\Delta P_{lowplenum}$ is the lower plenum pressure drop, ΔP_{core} is the core pressure drop, ΔP_{riser} is the riser pressure drop, $\Delta P_{topplenum}$ is the top plenum pressure drop, $\Delta P_{steamgenerator}$ is the steam generator pressure drop, and $\Delta P_{downcomer}$ is the downcomer pressure drop. The reversible pressure drops (i.e., accelerational pressure drop due to a flow area change or phase change) are canceled out as the momentum equation is integrated over the loop. The coolant mass flow in the primary loop is calculated utilizing Eq. (2) as one of the constraints.

3.1.1. 2Core pressure drop model

The total pressure drop in the core is formulated as follows:

$$\Delta P_{core} = \Delta P_{inlet} + \Delta P_{friction} + \Delta P_{spacer} + \Delta P_{outlet}, \tag{5}$$

where

$$\Delta P_{inlet} + \Delta P_{outlet} = (K_{inlet} + K_{outlet}) \frac{1}{2} \rho v^2, \tag{6}$$

$$K_{inlet} = 1; K_{outlet} = 0.42; \tag{7}$$

$$\Delta P_{fric} = f_{core} \frac{L_{core}}{D_e^{core}} \frac{1}{2} \rho v^2, \tag{8}$$

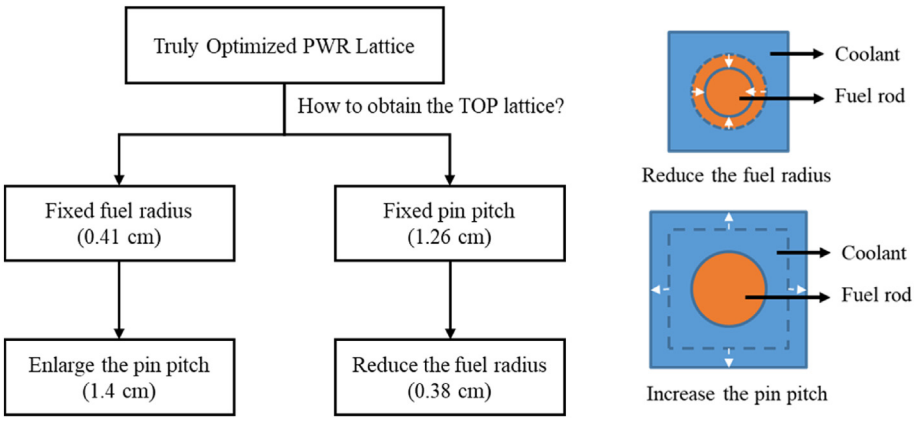

Fig. 2. Two TOP lattice configurations.

$$f_{laminar} = \frac{64}{\mathrm{Re}}, \tag{9}$$

$$\frac{1}{\sqrt{f_{turbulent}}} = -2\log\left(\frac{\varepsilon/D_h}{3.7} + \frac{2.51}{\mathrm{Re}\sqrt{f_{turbulent}}}\right), \tag{10}$$

$$\mathrm{Re} = \frac{\rho v D_e}{\mu}. \tag{11}$$

In the above equations, K is the form loss coefficient term for the coolant inlet and outlet, ρ is the coolant density, v is the coolant speed, f_{core} is the friction factor in the core, L_{core} is the core length, $f_{laminar}$ is the friction factor for laminar flow, $f_{turbulent}$ is the friction factor for turbulent flow utilizing Colebrook correlation [17], D_e^{core} is the equivalent core diameter, Re is the Reynold number, ε is the pipe surface roughness, D_h is the hydraulic diameter, v is the coolant flow speed, and μ is the fluid dynamic viscosity. The spacer pressure drop is calculated utilizing the Rehme's formula [18] as follows:

$$\Delta P_{spacer} = N_{spacer} C_v \left(\frac{\rho V_v^2}{2}\right)\left[\frac{A_s}{A_v}\right]^2, \tag{12}$$

where N_{spacer} is the number of the spacer grids, C_v is the drag coefficient, V_v is the average bundle fluid velocity, A_s is the projected frontal area of the spacer, and A_v is the unrestricted flow area. The drag coefficient C_v is calculated utilizing the Dalle Donne formulation [19] as follows:

$$C_v = \min\left[3.5 + \frac{73.14}{\mathrm{Re}^{0.264}} + \frac{2.79\times10^{10}}{\mathrm{Re}^{2.79}}, \frac{2}{\left[\frac{A_s}{A_v}\right]^2}\right]. \tag{13}$$

3.1.2. 2Steam generator pressure drop model

The NuScale core utilizes a Helical Coil-type Steam Generator (HCSG) as the PHX. Generally, there are two configurations of the HCSG tubes, which are in-line and staggered tube configurations. Fig. 3 describes both in-line and staggered tube configurations where S_L is the longitudinal pitch, S_T is the transversal pitch, u_{mean} is the average coolant speed, $u_{\max}$ is the maximum coolant speed, and d is the tube diameter.

In this study, the in-line tube configuration is assumed to be used in the HCSG. Therefore, the pressure drop of the primary coolant flow through the in-line tube configuration is calculated by utilizing the Gaddis-Gnielinski correlation [20] as follows:

$$\Delta P_{HCSG} = \xi N \frac{1}{2}\rho u_{max}^2, \tag{14}$$

$$u_{\max} = \frac{a}{a-1}u_{mean}, \tag{15}$$

where ξ is the drag coefficient, N is the number of tube columns, ρ is the coolant density, $u_{\max}$ is the maximum coolant velocity in the minimum cross-section area, u_{mean} is the average coolant velocity, and a is the transversal pitch to outer tube diameter ratio. The drag coefficient ξ is the summation of the drag losses due to the laminar flow (ξ_{lam}), turbulent flow (ξ_{turb}), inlet, and outlet effects (f_n). The drag coefficient is evaluated utilizing following equations:

$$\xi = \xi_{lam} + (\xi_{turb} + f_n)\left[1 - \exp\left(-\frac{\mathrm{Re}_d + 1000}{2000}\right)\right], \tag{16}$$

$$\xi_{lam} = 280\pi\frac{\left(b^{-0.5} - 0.6\right)^2 + 0.75}{a^{1.6}(4ab - \pi)\mathrm{Re}_d}, \tag{17}$$

$$\xi_{turb} = \frac{f_t}{\mathrm{Re}_d^{0.1\left(\frac{b}{a}\right)}}, \tag{18}$$

$$f_t = \left[0.22 + \frac{1.2\left(1 - \left(\frac{0.94}{b}\right)\right)^{0.6}}{(a-0.85)^{1.3}}\right]10^{0.47}\left(\frac{b}{a} - 1.5\right) + 0.03(a-1)(b-1), \tag{19}$$

$$f_n = \frac{1}{a^2}\left(\frac{1}{N} - \frac{1}{10}\right);\ \text{for } 5 \le N \le 10, \tag{20}$$

$$f_n = 0;\ \text{for } N \ge 10, \tag{21}$$

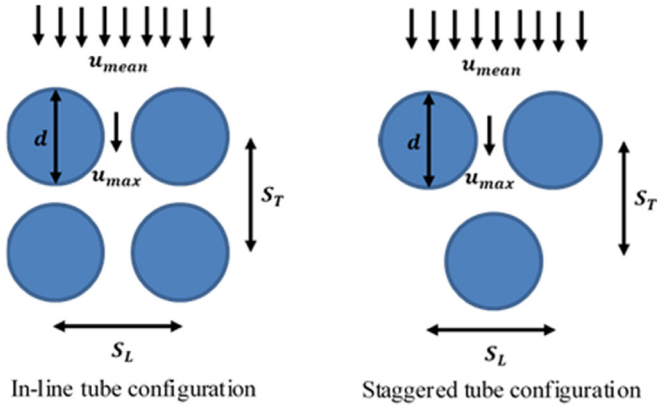

Fig. 3. In-line and staggered tube configuration.

$$D_e^{HCSG} = \begin{cases} \left(\frac{4a}{\pi} - 1\right)d; \text{ for } b > 1; \\ \left(\frac{4ab}{\pi} - 1\right)d; \text{ for } b < 1; \end{cases} \tag{22}$$

$$\mathrm{Re}_d = \frac{D_e^{HCSG} u_{\max} \rho}{\mu}, \tag{23}$$

where b is the longitudinal pitch to outer tube diameter ratio, Re is the Reynold number, d is the outer tube diameter, and μ is the coolant dynamic viscosity.

In the primary circulation loop, the friction pressure drops of the lower plenum, riser, upper plenum, and downcomer are much smaller than the pressure drops of the core and HCSG. Therefore, these pressure drops are neglected in this preliminary investigation while the form losses in those components are considered.

3.2. HCSG heat transfer model

The HCSG is comprised of the secondary coolant (water) flowing through the helical tubes while the primary coolant is on the shell side. In this preliminary investigation, the HCSG heat transfer is modelled with several simplifications utilizing the predetermined secondary side condition. The secondary system is not modelled explicitly, and the temperature at the secondary system is adjusted depending on the conditions. The objective of this model is to ensure that the HCSG heat transfer is equal to the generated reactor power. The HCSG heat transfer equation in steady state is given as follows:

$$G\frac{dh}{dz} = \frac{q'' P_h}{A_f}, \tag{24}$$

$$G\frac{\left(h\left(T_z^{primary}\right) - h\left(T_{z-1}^{primary}\right)\right)}{z_i - z_{i-1}} + \frac{\left(T_z^{primary} - T_z^{\sec ondary}\right)P_h}{R_{SG}A_f} \simeq 0, \tag{25}$$

where,

$$\frac{1}{R_{SG}} = \frac{Q}{A_h \Delta T_m}, \tag{26}$$

$$\Delta T_m = \frac{\Delta T_{\max} - \Delta T_{\min}}{\ln \frac{\Delta T_{\max}}{\Delta T_{\min}}}, \tag{27}$$

$$A_h = N_{tubes} P_h^{tubes} l, \tag{28}$$

$$P_h^{tubes} = \pi D_o, \tag{29}$$

where G is the mass flux, h is the coolant enthalpy, q'' is the heat flux, P_h is the heated perimeter, z is the HCSG axial mesh, A_f is the coolant flow area, R_{sg} is the steam generator thermal resistance, A_h is the total heat transfer area, Q is the total heat transferred to the secondary side, $\Delta T_{\max}$ and $\Delta T_{\min}$ are the maximum and minimum temperature difference between the primary and secondary sides, N_{tubes} is the total number of tubes, P_h^{tubes} is the helical tubes heated perimeter, l is the tube length, and D_0 is the outer diameter of the helical tubes. First, the HCSG thermal resistance R_{sg} is calculated utilizing the reference value and then used for the SG heat transfer calculation in Eq. (27). It is assumed that the heat transfers at the lower plenum, upper plenum, riser, and down-comer are negligibly small and neglected for the analysis.

3.3. Single channel model

Currently, the in-house Thermal-Hydraulic (TH) code is uncoupled with a neutronic code. Consequently, a chopped cosine function is used to determine the axial power distribution. Furthermore, the axial heat conduction is neglected, allowing the analysis to be performed at the axial level. First of all, the bulk temperature along the axial mesh is determined utilizing following equations:

$$h(z) = \frac{q'''(z)V_f}{w} + h(z-1), \tag{30}$$

$$T_b(z) = T_{hf}(h(z)), \tag{31}$$

where h is the coolant enthalpy, z is the axial mesh unit, V_f is the fuel volume unit, w is the single channel mass flow, T_b is the bulk temperature, and T_{hf} is the coolant temperature corresponding to the coolant enthalpy. Then, the evaluated bulk temperature distribution is utilized for the core pressure drop calculation in the single channel model and radial fuel temperature calculation. Finally, the heat conduction for the cylindrical fuel rod in the steady-state condition is calculated utilizing following equation:

$$\frac{1}{r}\frac{d}{dr}\left(kr\frac{dT}{dr}\right) + q'''(r) = 0, \tag{32}$$

where r is the fuel radius, T is the fuel temperature, k is the thermal conductivity, and q''' is the volumetric heat generation rate. Eq. (32) is solved by utilizing the standard Finite Difference Method (FDM). In determining the cladding (wall) temperature, the Dittus-Boelter correlation [21] and Jens-Lotte correlation [22] are utilized. The Dittus-Boelter and Jens-Lotte correlations are used for the sub-cooled and nucleate-boiling regions. The correlations are defined as follows:

Dittus-Boelter:

$$Nu = 0.023\mathrm{Re}^{0.8}\mathrm{Pr}^{0.4}, \tag{33}$$

$$Nu = \frac{h_c D_e}{k_f}, \tag{34}$$

$$h_c = \frac{q''}{T_w - T_b}. \tag{35}$$

Jens-Lotte:

$$\frac{q''(W/m^2)}{10^6} = \frac{\exp\left(\frac{4P(Pa)}{6.2\times10^6}\right)}{25^4}(T_w(C) - T_{sat}(C))^4, \tag{36}$$

where Nu is the Nusselt number, Re is the Reynold number, h_c is the convective heat transfer coefficient, k_f is the fluid thermal conductivity, D_e is the equivalent diameter, Pr is the Prandtl number, q'' is the heat flux, P is the coolant pressure, T_w is the wall temperature, and T_{sat} is the saturated coolant temperature. The estimated temperatures from both correlations are compared, and the lower value will be used as the wall temperature.

3.4. Calculation algorithm

The in-house code reads the input data regarding the system geometry, power parameter, and other necessary data. First, the buoyancy pressure head and initial total mass flow rate are determined. Then, the code performs the primary system pressure drop evaluation following the primary circulation loop. Then, the total mass flow rate is updated and evaluated utilizing Eq. (2). The reactor power is calculated after the mass flow rate converges. The detailed calculational flow chart is shown in Fig. 4.

4. Numerical results and discussions

The NuScale reactor core is designed based on the 17 × 17 PWR FA with 160 MWth power for one Nuclear Power Module (NPM) [11]. The HCSG is utilized as the primary heat exchanger. The reactor pressure vessel height is 17.7 m and the diameter is 2.7 m, containing the reactor core, pressurizer, and HCSG. Table 1 shows the main parameters of the NuScale reactor design considered in this work.

Fig. 5 shows the primary coolant flow pattern in the NuScale SMR system [23]. The current analysis considers the lower plenum, core, riser, upper plenum, HCSG, and downcomer. Detailed information regarding the NuScale reactor design can be found further in references [11,23,24].

As the NuScale licensing process is ongoing with the target to be a commercial reactor, several key parameters, especially for the HCSG, are not available to the public. Therefore, several assumptions are utilized in this study. First, the thermal center difference is approximated as the distance between the active core center and the HCSG center, which is 8.354 m. As the coolant temperature difference between the inlet and exit is known, the buoyancy force of the NuScale core is calculated utilizing Eq. (3). Based on Eq. (2), the buoyancy force is equivalent to the total system pressure drop

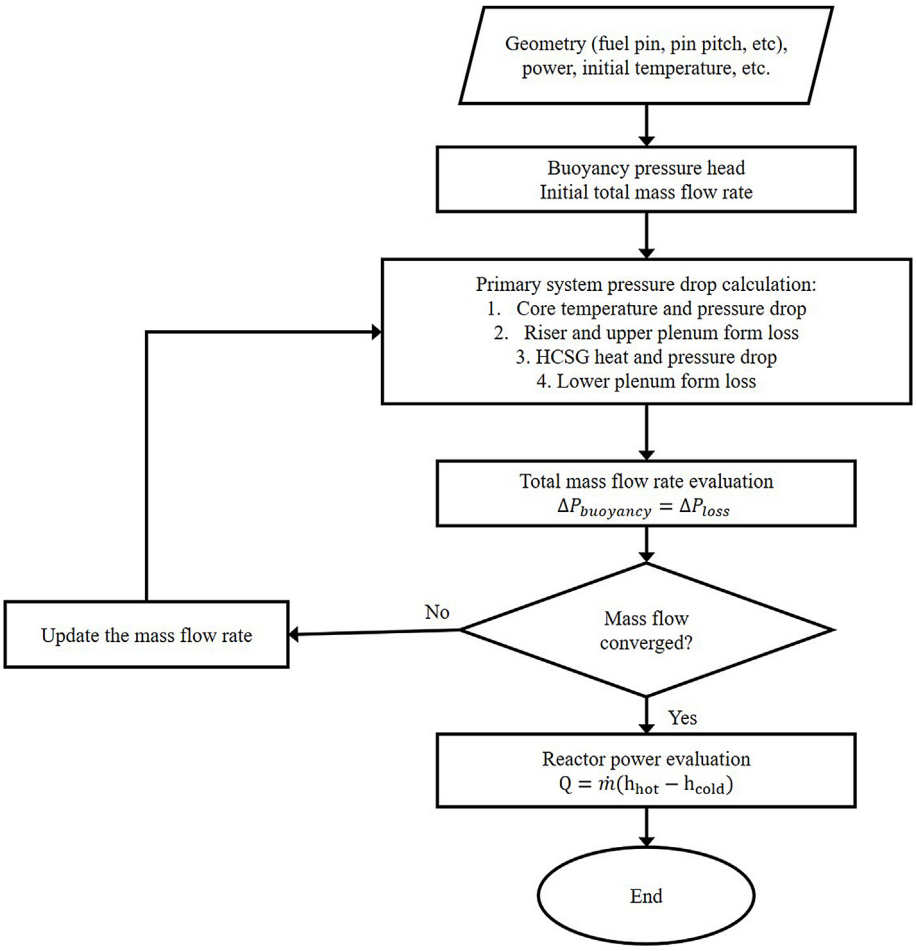

Fig. 4. The calculation flow chart.

Table 1
Major design parameters of the NuScale reactor [11].

Parameter	Value
Core power	160 MWth
Height of active core	2 m
System pressure	12.75 MPa
Inlet temperature	531.5 K
Best estimate flow	587.15 kg/s
Average core coolant velocity	0.82 m/s
Number of FA	37
FA pitch	21.5 cm
Fuel rod pitch	1.26 cm
Fuel rod diameter	0.95 cm
Fuel density	10.625 g/cm^3
Number of spacer grids per FA	5
Number of helical tubes per NPM	1380
Tube column per NPM	21
Steam temperature	579.8 K
Feedwater temperature	422 K
HCSG tube outer diameter	15.875 mm
HCSG total heat transfer area	1665 m^2
Total primary coolant flow path	2673 cm

in the steady-state condition. In addition, the ratio of core pressure drop to the total system pressure drop $P_{drop}^{core}/P_{drop}^{total}$ is assumed to be 0.3. By utilizing these two constraints, the whole analysis regarding the pressure drop can be performed.

Table 2 shows the numerical results for the reference design and both TOP lattice designs. First, the in-house code is utilized to perform the calculation for the standard reference design to validate the assumptions. The P_{drop}^{other} comprises of the lower plenum, upper plenum, riser, and downcomer form loss. It is found that the

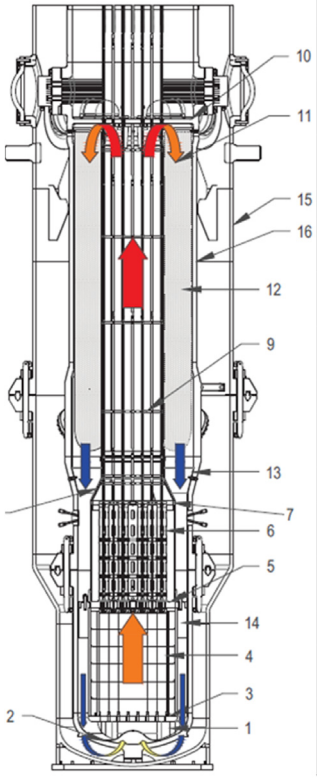

No.	Description
1	Core support blocks in downcomer
2	Downcomer to lower plenum turn
3	Core support blocks in downcomer
4	Upper core plate
5	Core support blocks in downcomer
6	Control rod assembly guide tubes
7	Control rod assembly guide tube support plate
8	Riser transition
9	Control rod dive shaft support
10	Pressurizer baffle
11	Upper riser turn to annulus
12	Downcomer through steam generator
13	Downcomer transition
14	Upper core support block
15	Containment vessel
16	Reactor vessel

Fig. 5. NuScale primary coolant circulation loop [23].

in-house code results are close to the reference ones, while the average core coolant velocity is a bit overestimated. By utilizing the reference mass flow rate, average core temperature, and core flow area, the average core coolant velocity is estimated to be 0.868 m/s. The slight difference in the coolant speed might be due to the core bypass flow, which is not considered in the current analysis. The core mass flow rate, thermal power, and hot and cold leg temperatures are similar to the reference values. Therefore, the single channel analysis model and other utilized assumptions are considered to be acceptable and can be used to analyze the TOP lattice impacts.

The TOP design analysis is performed using identical inlet and outlet temperatures as the constraint. For simplicity, the TOP design configuration is identified by the pin pitch followed by the fuel pellet radius, and the units are in cm. For example, 1.26/0.38 means that the TOP design pin pitch is 1.26 cm and the fuel pellet radius is 0.38 cm.

Fig. 6 shows the impacts of the TOP lattice designs compared to the standard reference FA design. It is observed that the core coolant flow area dictates the impacts of the TOP design on the core. The core pressure drop is reduced by enlarging the core coolant flow area, increasing the mass flow rate and core thermal power. The thermal power increases by 2.5% and 9.8% for the 1.26/0.38 and 1.40/0.41 TOP designs, respectively. The 1.26/0.38 design thermal power gain is much smaller than that of the 1.40/0.41 design due to the smaller increase of the core coolant flow area, resulting in a smaller decrease in the core pressure drop. The increase in thermal power is proportional to the increase in mass flow rate under the same ΔT constraint. As the core pressure drop decreases and the mass flow rate increases, the HCSG pressure drop and the other loss form pressure drops increase, satisfying the steady-state natural circulation condition. Additionally, the core coolant speed is reduced due to the increase of the coolant flow area in the core. Generally, the Critical Heat Flux (CHF) is a function of the pressure, quality, coolant enthalpy (inlet and saturated), and coolant mass flux. The mass flux itself is the function of the core coolant speed. Therefore, the CHF and the Departure from Nucleate Boiling Ratio (DNBR) value might be lower due to the reduced core coolant speed. The core coolant speed reduction of the 1.26/0.38 TOP design is clearly smaller than the 1.40/0.41 design. Consequently, the DNBR reduction of the 1.26/0.38 design should be lower than the 1.40/0.41 design. However, it should be noted that the CHF is also a function of the pressure, quality, and coolant enthalpy. Therefore, a comprehensive TH-analysis is necessary to advocate the benefits of both TOP designs.

One of the primary assumptions in this study is the ratio of the core pressure drop to the total system pressure drop. Consequently, a sensitivity study regarding the $P_{drop}^{core}/P_{drop}^{total}$ ratio is performed. In the results of Table 2, it is assumed that the ratio of the core pressure drop to the total pressure drop is 0.3. For the sensitivity analysis, the ratio is perturbed by ± 0.05.

Figs. 7 and 8 show the sensitivity results for the 1.26/0.38 TOP design and 1.40/0.41 TOP design, respectively. One notes that both TOP designs exhibit similar behavior in the sensitivity analysis. It is clear that the power gain is more significant with a bigger $P_{drop}^{core}/P_{drop}^{total}$ ratio in both TOP designs. Meanwhile, as the $P_{drop}^{core}/P_{drop}^{total}$ ratio increases, the reduction of the core pressure drop has a more significant impact on increasing the mass flow and thermal power due to the bigger weighting of the core pressure drop. Therefore, even though the reduction of the core pressure drop at 0.25 $P_{drop}^{core}/P_{drop}^{total}$ ratio is the biggest, the thermal power gain is the smallest.

Finally, one of the essential parameters in the reactor design is the MTC. As discussed in the introduction and TOP lattice section, a

Table 2
Impacts of the standard and TOP lattice on the reactor performance.

Parameter	Pin pitch/fuel radius (cm)		
	1.26/0.41	1.26/0.38	1.40/0.41
Equivalent core radius (cm)	73.78	73.78	81.95
$P_{drop}^{core}(Pa)$	2353	2085	1276
$P_{drop}^{HCSG}(Pa)$	5070	5315	6056
$P_{drop}^{other}(Pa)$	444	467	535
Mass flow (kg/s)	587 (587.15)[a]	602	645
Average core coolant speed (m/s)	0.87 (0.82)[a]	0.83	0.66
Core coolant flow area (m^2)	245	265	354
$T_{coolant}^{hot}(^{\circ}C)$	310 (310)[a]	310	310
$T_{coolant}^{cold}(^{\circ}C)$	259 (259)[a]	259	259
Thermal power (MWth)	160	164	175

[a] Reference values.

sufficiently negative and similar MTC throughout the reactor operation is preferable for a smaller temperature defect and larger cold shutdown margin, especially in the highly burned condition. The MTC analysis is performed for each fuel assembly type utilizing the Serpent 2 Monte Carlo code with ENDF/B-VII.1 library [25,26]. A standard 17 × 17 FA configuration without burnable absorbers is considered for a consistent comparison. Table 3 shows the MTC comparison of each FA type at 0 MWd/kgU and 40 MWd/kgU, including the MTC uncertainty.

It is observed that the standard FA design has the most negative MTC and also the biggest MTC changes during the FA depletion. The standard PWR FA design is optimized under the soluble boron condition to assure a negative MTC throughout the reactor operation. Therefore, the fuel lattice is clearly under-moderated, resulting in a strongly negative MTC, which may affect the stability of the reactor axial power. Meanwhile, both TOP FA designs are optimized

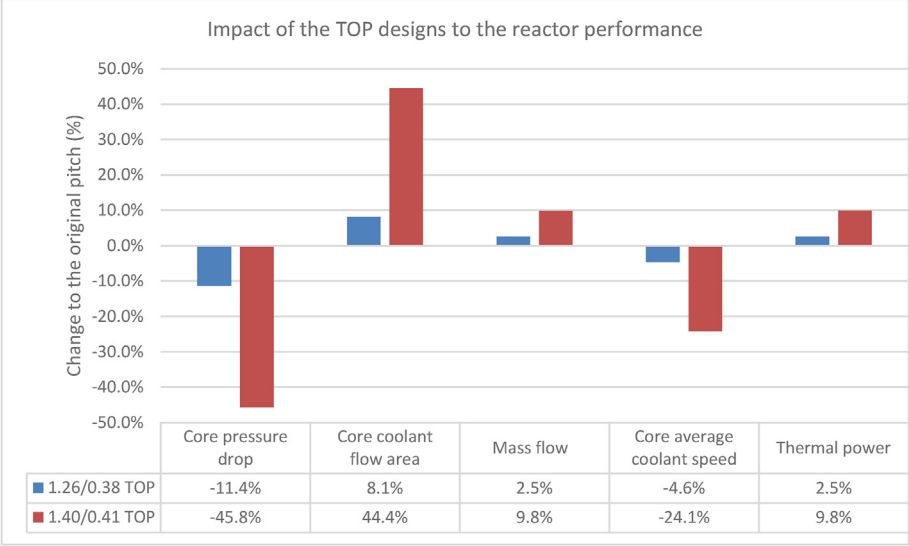

Fig. 6. Comparison of each TOP design's impact on the reactor performance.

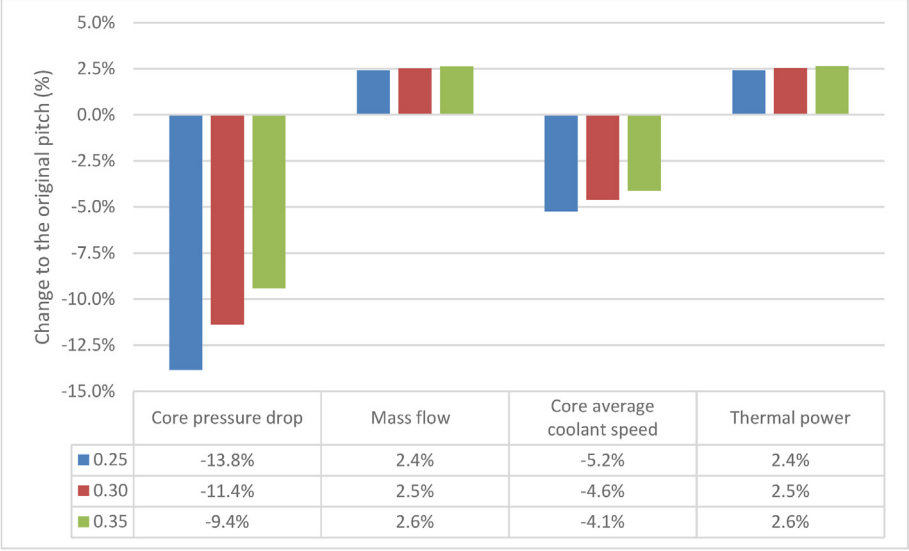

Fig. 7. Sensitivity analysis for the 1.26/0.38 TOP design.

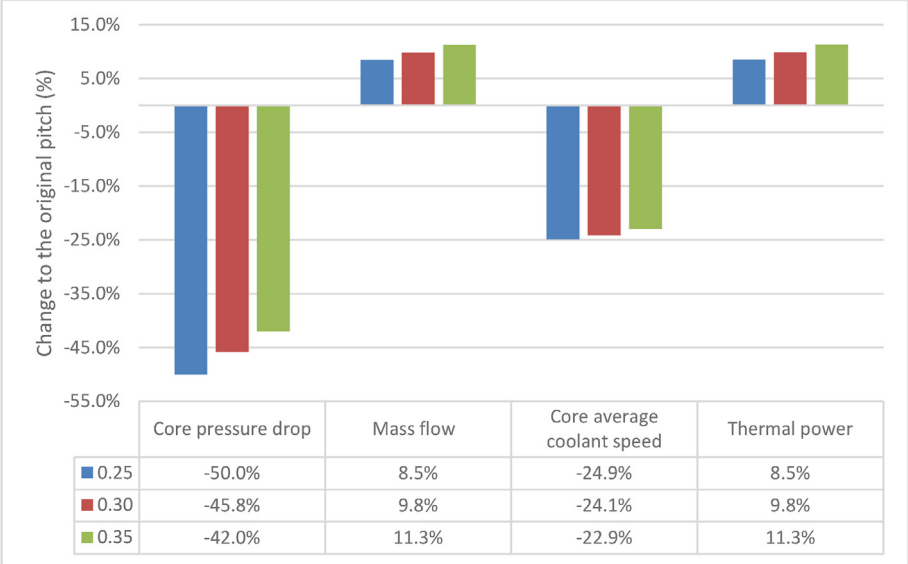

Fig. 8. Sensitivity analysis for the 1.40/0.41 TOP design.

Table 3
The MTC comparison between the standard and TOP FAs.

FA design	H/U	0 MWd/kgU		40 MWd/kgU		MTC changes (pcm/K)
		MTC (pcm/K)	Uncertainty (pcm/K)	MTC (pcm/K)	Uncertainty (pcm/K)	
Standard PWR FA	4.10	−30.39	0.32	−40.55	0.43	−10.16
TOP 1.26/0.38	5.25	−24.90	0.30	−29.56	0.40	−4.66
TOP 1.40/0.41	6.28	−18.29	0.28	−21.63	0.38	−3.35

to have a softer neutron spectrum resulting in sufficiently negative MTC and minor MTC changes during the depletion.

5. Conclusions

This study focuses on the investigation of the TOP design impacts on the natural circulation SBF SMR. It is found that the core coolant flow area is the main parameter that dictates the impact of the TOP lattice design to the reactor performance. The thermal power increases by 2.5% and 9.8% for 1.26/0.38 and 1.40/0.41 TOP lattices, respectively. The bigger power gain of the 1.40/0.41 design is due to the more significant increase in the core's coolant flow area. In terms of the core average coolant speed, the 1.26/0.38 design has a smaller reduction than the 1.40/0.41 design, indicating that the reduction of the CHF and DNBR might be lower too. The utilization of the 1.26/0.38 design is also suitable for the existing core without a change in the reactor size.

Furthermore, the possibly thermal power gain is bigger in the proposed TOP designs with the increase of the core fractional pressure drop. Additionally, as the fractional pressure drop in the core increases, the reduction of the core pressure drop has a more significant effect on the thermal power gain. Finally, it is confirmed that both TOP designs have a sufficiently negative and similar MTC throughout the depletion. In contrast, the standard FA design has strongly negative and significant MTC changes in highly burned conditions.

A comprehensive TH-analysis using a 3D power profile must be performed to justify the benefits of the TOP design and determine the optimized design in terms of both neutronic and thermal-hydraulics viewpoints. In addition, the pressure drop model should also be refined further for more accurate results.

Declaration of competing interest

The authors declare that they have no known competing financial interests or personal relationships that could have appeared to influence the work reported in this paper.

Acknowledgment

This work was supported by the National Research Foundation of Korea (NRF) Grant funded by the Korean Government (MSIP) (NRF-2016R1A5A1013919).

Abbreviation

ATOM	Autonomous Transportable On-demand Reactor Module
CHF	Critical Heat Flux
CVCS	Chemical and Volume Control System (CVCS)
DNBR	Departure from Nucleate Boiling Ratio
FA	Fuel Assembly
FDM	Finite Difference Method
HCSG	Helical Coil Steam Generator
HTU	Hydrogen-to-Uranium
LOCA	Loss of Coolant Accident
MTC	Moderator Temperature Coefficient
PHX	Primary Heat Exchanger
SBF	Soluble-Boron-Free
SMR	Small Modular Reactor
TH	Thermal-Hydraulic
TOP	Truly Optimized PWR

References

[1] M.K. Rowinski, T.J. White, J. Zhao, Small and medium-sized reactors (SMR): a review of technology, Renew. Sustain. Energy Rev. 44 (2015) 643–656.
[2] EPRI, Elimination of Soluble Boron for a New PWR Design, Report Document EPRI-NP-6536, 1989.
[3] M.S. Yahya, H. Yu, Y.H. Kim, Burnable absorber-integrated Guide Thimble (BigT) – I: design concepts and neutronic characterization on the fuel assembly benchmarks, J. Nucl. Sci. Technol. 53 (7) (2016) 1048–1060.
[4] A.E. Abdelhameed, H.U. Rehman, Y. Kim, A physics study for passively-autonomous daily load-follow operation in soluble-boron-free SMR, in: International Congress on Advanced Nuclear Power Plants, Fukui & Tokyo, Japan, 2017.
[5] A.E. Abdelhameed, X.H. Nguyen, Y. Kim, Feasibility of passive autonomous frequency control operation in a Soluble-Boron-Free small PWR, Ann. Nucl. Energy 116 (2018) 319–333.
[6] J. Liman, Small modular reactors: methodology of economic assessment focused on incremental construction and gradual shutdown option, Prog. Nucl. Energy 108 (2018) 253–259.
[7] X.H. Nguyen, S. Jang, Y. Kim, A spectral optimization study of fuel assembly for soluble-boron-free SMR, in: Transaction of the Korean Nuclear Society Spring Meeting, 2020. Jeju, South Korea.
[8] X.H. Nguyen, S. Jang, Y. Kim, Impacts of an ATF cladding on neutronic performances of the soluble-boron-free ATOM core, Int. J. Energy Res. 44 (2020) 8193–8207.
[9] N.E. Todreas, et al., NUCLEAR SYSTEMS II Elements of Thermal Hydraulic Design, Taylor and Francis, 2001.
[10] P. Zhao, et al., Code development on steady-state thermal-hydraulic for small modular natural circulation lead-based fast reactor, Nucl. Eng. Technol. 52 (12) (2020) 2789–2802.
[11] NuScale Inc, Final Safety Analysis Report – Part 02 – Tier 02- Chapter 04-reactor, 2020.
[12] S. Wijaya, X.H. Nguyen, Y. Kim, A Study on Natural Circulation Soluble-Boron-Free SMR with Long Cycle and High Burnup, Transaction of American Nuclear Society Virtual Annual Meeting, 2021.
[13] S. Wijaya, X.H. Nguyen, Y. Kim, An Investigation of Three-Batch Fuel Management in a Natural Circulation Soluble Boron Free SMR, Transaction of American Nuclear Society Winter Meeting, 2021.
[14] X.H. Nguyen, S. Jang, Y. Kim, Truly-optimized PWR lattice for innovative soluble-boron-free small modular reactor, Sci. Rep. 11 (2021), 12891.
[15] S. Wijaya, Y. Kim, Impact of truly optimized PWR lattice on maximum power of natural circulation reactor, in: Transaction of the Korean Nuclear Society Virtual Autumn Meeting, 2020.
[16] K. Song, K. Jeon, Y. Jang, J. Park, Y. Koo, Progress in nuclear fuel technology in Korea, Nucl. Eng. Technol. 41 (4) (2009) 493–520.
[17] C.F. Colebrook, Turbulent flow in pipes with particular reference to the transition region between the smooth and rough pipe laws, J. Insitute Civil Eng. 11 (4) (1930) 133–156.
[18] K. Rehme, Pressure drop correlations for fuel elements spacers, Nucl. Technol. 17 (1973) 15–23.
[19] D. Donne, et al., Thermohydraulic optimization of homogeneous and heterogenous advanced pressurized reactors, Nucl. Technol. 80 (1988) 107–132.
[20] E.S. Gaddis, V. Gnielinski, Pressure drop of tube bundles in cross flow, Int. Chem. Eng. 25 (1985) 1–15.
[21] F.W. Dittus, L.M.K. Boelter, Heat Transfer in Automobile Radiators of the Tubular Type, vol. 2, University of California Publications in Engineering, 1930, pp. 443–461.
[22] W.H. Jens, P.A. Lottes, Analysis of Heat Transfer, Burnout, Pressure Drop and Density Data for High Pressure Water, Argonne National Laboratory, 1951. ANL-4627.
[23] NuScale Inc., Final safety analysis report - part 02 - tier 02- (chapter 05)-reactor coolant system and connecting system., 2020.
[24] F. Patrick, Transient Thermal-Hydraulic Simulation of a Small Modular Reactor in Relap 5", Master's Theses, University of Rhode Island, Kingston, 2018.
[25] J. Leppanen, et al., The Serpent Monte Carlo code: status, development and applications in 2013, Ann. Nucl. Energy 82 (2015) 142–150.
[26] M.B. Chadwick, et al., ENDF/B-VII.1 nuclear data for science and technology: cross sections, covariances, fission product yields and decay data, Nucl. Data Sheets 112 (2011) 2887–2996.